

## **ELECTROMAGNETIC LOSSES IN MAGNETIC SHIELDS FOR BURIED HIGH VOLTAGE CABLES**

**P. Sergeant** <sup>†</sup>

Department of Electrical Energy, Systems and Automation  
Ghent University, Ghent B-9000, Belgium

**S. Koroglu**

Department of Electrical & Electronics Engineering  
Faculty of Engineering, Pamukkale University  
Denizli 20070, Turkey

**Abstract**—The electromagnetic losses and shielding efficiency of shields for a buried three phase high voltage cable are studied for several shielding configurations. The shields are U-shaped gutters covered with plates, and the power cables are positioned either in trefoil or in flat configuration. The shielding efficiency and the losses are compared for shields with the same geometry but several shielding materials: aluminium, and two ferromagnetic steel grades. The numerical models are validated with experimental results. From the experiments, it is observed that the average reducing factor of the flux density is about 7 with the flat cable configuration while the average reducing factor of the flux density is about 5 with the trefoil cable configuration. But the power losses in the DX52 shield for trefoil configuration is about 40% lower compared to the flat configuration. In case of trefoil configuration, the losses are 12.14 W/m per meter length in the shield for a current of 750 A. Next to the shield material and the cable configuration, the paper investigates the influence of several parameters on both the shielding efficiency and the losses: the size of the shield, the current amplitude in the cable and the thickness of the shield.

---

*Received 22 February 2011, Accepted 6 April 2011, Scheduled 13 April 2011*

Corresponding author: Selim Koroglu (skoroglu@pau.edu.tr).

<sup>†</sup> Also with Department of Electrotechnology, Faculty Applied Engineering Sciences, University College Ghent, Ghent B-9000, Belgium.

## 1. INTRODUCTION

Extremely low frequency (ELF) magnetic fields cause a considerable disturbance of the operation and accuracy of sensitive electrical and electronic equipment [1] and may cause health hazards for human beings [2,3]. The exposure limit values may change from country to country. They are regulated by law or by communities, and have a tendency to decrease more and more. We consider the levels of the European community, in particular the recommendation for field exposure limits for the general public [4]. Examples of ELF sources are, e.g., power cables, switchyards, substations, and industrial and transformer centres. Especially, the buried high voltage and underground cables have drawn a great deal of attention recently. To reduce the magnetic field produced by the magnetic sources, several methods have been proposed such as phase arrangement in the power cables [5, 6], compensating passive loops [7, 8], and shielding by conductive or ferromagnetic materials [9, 10].

A lot of shield structures and configurations can be used in the magnetic shielding for buried cables such as open and closed shield configurations. According to [9], it can be concluded that open shield configurations (e.g., flat sheets above buried cables) can have good shielding performance if they are large, thick and if there is a minimal distance between the cables and the shield. Furthermore, in [11], a much better shielding efficiency is found for closed shields than for open shield configurations. The literature describes several possible closed shield structures for three-phase cables: a steel pipe [12], an infinitely long cylinder of hexagonal cross-section which is a longitudinal juxtaposition of two doubly bent laminations [10], and U-shaped gutters covered with plates [9, 13].

In [14], a hybrid method based on unimoment method is presented for investigating the electromagnetic shielding of sources within a steel pipe or a tube made of ferromagnetic material. In [15], the eddy-current loss was calculated with regard to balanced and unbalanced currents in a pipe-type cable using a numerical method (FEM). In [16], an analytical solution is presented for the approximation of losses in a steel casing with multiple cables inside the pipe and an arbitrary cable arrangement. The analytical method is based on the theory of images and on the method of filaments. In addition, the iron power losses can be calculated according to the statistical theory [17] in the soft magnetic materials.

Therefore, it is interesting to investigate a closed shield configuration consisting of a U-shaped gutter with a flat cover plate (Fig. 1 and Table 1) because maintenance and repair operations

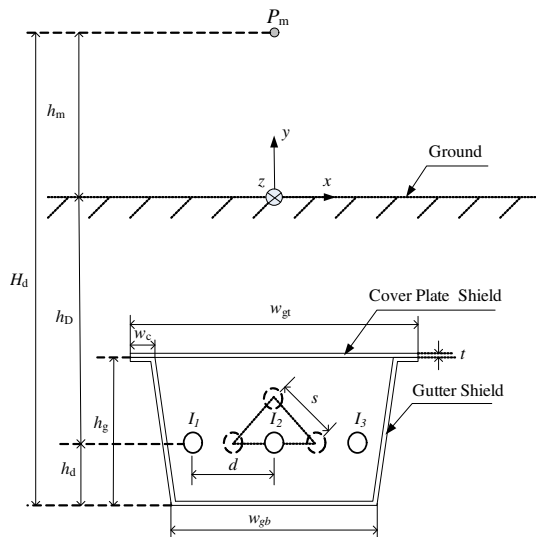


**Figure 1.** Geometry in the  $xy$ -plane of the buried HV cables and the shielding configuration.

can be done easily. Furthermore, if we make a good shielding, we should consider not only shielding efficiency but also power losses in the shield as well as shield cost. This paper investigates electromagnetic losses in magnetic shielding for HV cables. The shield losses are studied for three materials with 3 mm thickness: two electrically conducting and ferromagnetic shielding materials with nonlinear hysteretic behavior (Magnetil and DX52, both from Arcelor-Mittal), and a non-ferromagnetic and electrically conducting shielding material (aluminium). The shield geometry consists of U-shaped gutters covered with plates in the same material. This allows the readers to choose which material is the best for a given shielding problem.

The paper focuses both on the shielding performance and on the losses in the shield. A good shield should have both a high shielding efficiency and low electromagnetic losses. We are convinced that both aspects should be studied together.

## 2. MAGNETIC SHIELDING OF THE BURIED HIGH VOLTAGE CABLES

The goal of the research is to find both the best shielding factor and the lowest power losses in the shield. The geometry of the studied

**Table 1.** Dimensions of shielding configuration for simulation and for experimental setup at reduced scale.

| Quantity        | Simulation             | Experiment           | Description   |
|-----------------|------------------------|----------------------|---|
| $h_m$           | 1.00 m                 | 0.25 m               | Height of evaluation points                                       |
| $h_D$           | 1.30 m                 | 0.650 m              | Distance from the ground surface to the origin of cables          |
| $h_d$           | 0.20 m                 | 0.10 m               | Distance from the centre of the cable to the bottom of the gutter |
| $H_d$           | 2.00 m                 | 1.00 m               | Distance from the observation points to the bottom of the gutter  |
| $h_g$           | 0.532 m                | 0.266 m              | Height of the gutter  |
| $w_{gt}$        | 1.040 m                | 0.520 m              | Width of the bottom of the gutter and the cover plate             |
| $w_{gb}$        | 0.650 m                | 0.325 m              | Width of the top of the gutter                                    |
| $w_c$           | 0.10 m                 | 0.05 m               | Width of the gutter clips   |
| $t$             | 3 mm                   | 3 mm                 | Thickness of the shield   |
| $d$             | 0.20 m                 | 0.10 m               | Distance between the cables for the flat configuration            |
| $s$             | 0.20 m                 | 0.10 m               | Distance between the cables for the trefoil configuration         |
| $I_1, I_2, I_3$ | 1500 A (rms)           | 750 A (rms)          | Phase current amplitude   |
| $A$             | **1600 mm <sup>2</sup> | *250 mm <sup>2</sup> | Cross section area of the cables                                  |

\*\* We used a round cable cross section during the simulation, with a cable radius of 22.57 mm.

\* We used a rectangular cable cross section (a bus bar) in the experimental setup, with a copper section width of 5 mm and a copper section height of 50 mm.

shielding application is shown in Fig. 1. Table 1 gives the dimensions, on the one hand of the simulated real application, and on the other hand of the reduced scale experiment. The shielded region is outside the shield, above the ground surface. The source region is inside in the shield.

The goal is to study the shielding efficiency that is defined in dB in a point as:

$$SE = 20 \log_{10} (|B_0| / |B_s|), \quad (1)$$

where  $B_0$  is the magnetic field density without shield present and  $B_s$  is the magnetic field density in the same point with shield.

### 3. MODELS

#### 3.1. FEM Model

The 2-D Finite element model (FEM) is a time-harmonic model with the vector potential  $\bar{A}$  as unknown. The model can be defined as:

$$\nabla \times \left( \frac{1}{\mu} \nabla \times \bar{A} \right) + j\omega\sigma\bar{A} = \bar{J}_e, \quad (2)$$

here,  $\omega$  is the angular frequency,  $\sigma$  is the conductivity,  $\bar{J}_e$  is external current density, and  $\mu$  is the permeability which is a function of the flux density to model hysteresis and nonlinearity for the ferromagnetic materials. In the case of nonlinearity, the FEM requires iterative solving. The 2-D FEM has typically 137881 degrees of freedom. An example of the 2D FEM mesh structure with trefoil cable and the shield configuration is shown in Fig. 2. We used the commercial software package Comsol. The parametric studies were programmed in a Matlab environment with an interface to Comsol.

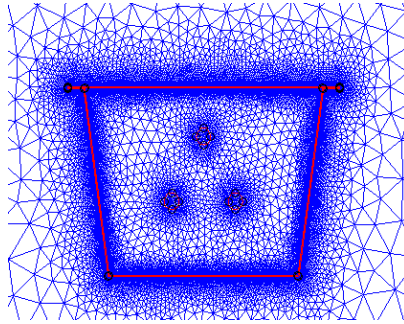


**Figure 2.** An example of 2D FEM mesh structure of the trefoil cable and the shield configuration.

We consider three types of shielding material during the FEM simulation for the shielding application: two electrically conducting and ferromagnetic shielding materials (Magnetil and DX52), and a non-ferromagnetic and electrically conducting shielding material (Aluminium). The first two materials use a nonlinear constitutive law obtained from hysteresis loop measurements on strips of the shielding material with nonlinear hysteretic behavior in an Epstein frame. Loops were measured at 0.5 Hz for DX52, at 0.2 Hz for the Magnetil material, and the single valued characteristics were found from the peak values of  $H$  and  $B$ . Fig. 3 shows the characteristic

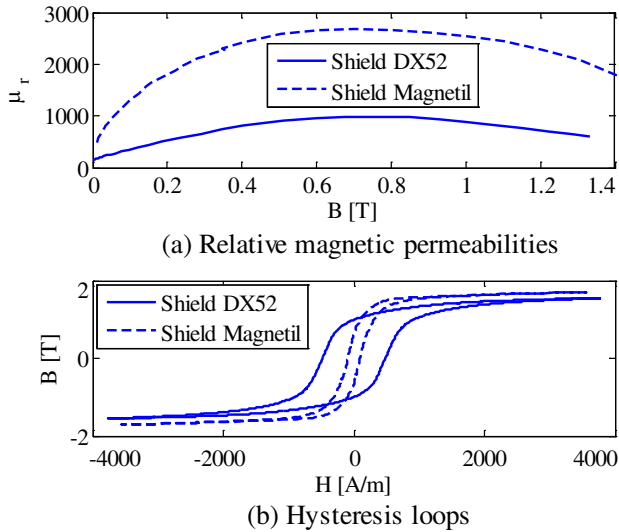


**Figure 3.** (a) Relative magnetic permeabilities as a function of the magnetic flux density. (b) Hysteresis loops in the  $BH$  plane at 0.5 Hz for DX52 and 0.2 Hz for Magnetil.

of the magnetic permeabilities  $\mu(B)$  and measured hysteresis loops in the  $BH$  plane for these ferromagnetic shielding materials: a rather high quality grade with high permeability and low hysteresis loss (Magnetil), and a cheaper grade with lower permeability and higher hysteresis loss (DX52).

The electrical conductivities  $\sigma$  were obtained from a 4-point measurement on a rectangular sample of the shield materials. The value is 6.48 MS/m and 8.50 MS/m for DX52 and Magnetil, respectively. The densities are 7580 kg/m<sup>3</sup> for DX52, 7800 kg/m<sup>3</sup> for Magnetil. And also, as a non-ferromagnetic and electrically conducting shielding material we consider a typical aluminium alloy for eddy currents applications, with relative magnetic permeability  $\mu_r = 1$ , conductivity  $\sigma = 36$  MS/m, density = 2700 kg/m<sup>3</sup>.

### 3.2. Loss Model

The iron losses in soft magnetic materials can be separated into three components; hysteresis losses, classical losses and excess losses [18–20]. The total losses  $P$  are:

$$P = P_h + P_c + P_e, \quad (3)$$

where  $P_h$ ,  $P_c$  and  $P_e$  are hysteresis, classical (eddy current), and excess losses, respectively.

The several loss contributions for the two electrically conducting and ferromagnetic shielding materials are shown in Fig. 4. The hysteresis losses are found from low frequency hysteresis loop measurements. As a consequence of the relatively high thickness of the strips, a frequency of 0.2 Hz was chosen to minimize eddy currents in the laminations. It can be observed from Fig. 4(c) that DX52 has about 3 times more hysteresis loss than Magnetil. The shape of the quasi-static loops in Fig. 3(b) shows the much higher coercive field of DX52, as well as the much lower permeability. The reason to choose these two materials with equal thickness of 3 mm, is to compare the “high quality” Magnetil, designed for shielding applications, with a cheap hot rolled steel DX52.

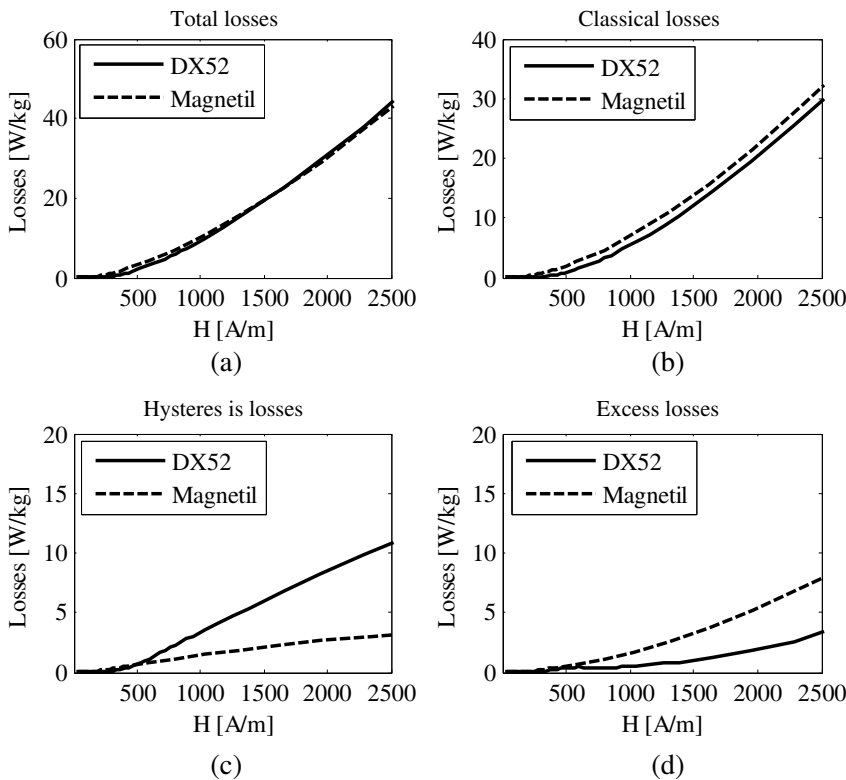


**Figure 4.** Power loss contributions for two electrically conducting and ferromagnetic shielding materials: Magnetil and DX52.

The classical losses can be computed in the strip with known dimensions. This was done with a 2D FEM of the strip cross section. The measured electrical conductivity and the static  $BH$ -characteristic were implemented as properties. The magnetic field is imposed at the edges of the material. Notice that the often used formula  $\pi^2/6\sigma d^2 f^2 B^2$  is not valid for the frequency of 50 Hz (or higher) because the penetration depth is smaller than (half of) the material thickness. Given the high lamination thickness, the classical losses are the dominant loss contribution: Fig. 4(b).

The excess loss is obtained by measuring the total losses of dynamic  $BH$ -loops, and subtracting the hysteresis and classical loss. The excess loss is low for the considered materials: Fig. 4(d).

## 4. SIMULATION RESULTS

### 4.1. Without Shielding

The low-frequency magnetic field produced by buried high-voltage (HV) cables can reach levels of a few  $\mu\text{T}$  or more, close to the cable. The magnetic induction level depends on the currents in the cables, the distance from the cables, the distance between the conductors and the cable configuration. In the case without shield, the simulations have been carried out for the trefoil and flat cable configurations and several distances between the cables. Fig. 5 shows the variation of the magnetic flux density along the  $x$ -axis for several distances between the cables, which are in (a) flat and (b) trefoil configuration. As a function of the distance between the cables, the induction level is calculated at  $h_m = 1$  m above the surface of the ground, for a nominal current of 1500 A rms per phase and for flat and trefoil cable configurations. From Fig. 5, it is observed that the magnetic flux density values depend on the distance between cables and the cable configuration. For the flat configuration, the maximum induction value is 24.29  $\mu\text{T}$  for  $d = 0.3$  m and 8.21  $\mu\text{T}$  for  $d = 0.1$  m. The trefoil cable configuration gives a better reduction of the magnetic flux density than the flat configuration. For example, the average reduction of the magnetic field density for the trefoil configuration is 13% better than a flat configuration in the case without shield, where the same distance  $s = d = 0.2$  m between the cables is considered for both cable configurations.

Additionally, the magnetic flux density distribution along the  $x$ -axis for the trefoil configuration ( $s = 0.20$  m) at several heights  $h_m$  is shown in Fig. 6. From Fig. 6, it is observed that the magnetic field level strongly depends on the height of the evaluation points. For example, the maximum of the flux density levels is found to be 47.41  $\mu\text{T}$  and 9.75  $\mu\text{T}$  at  $h_m = 0$  m and  $h_m = 1.5$  m, respectively.

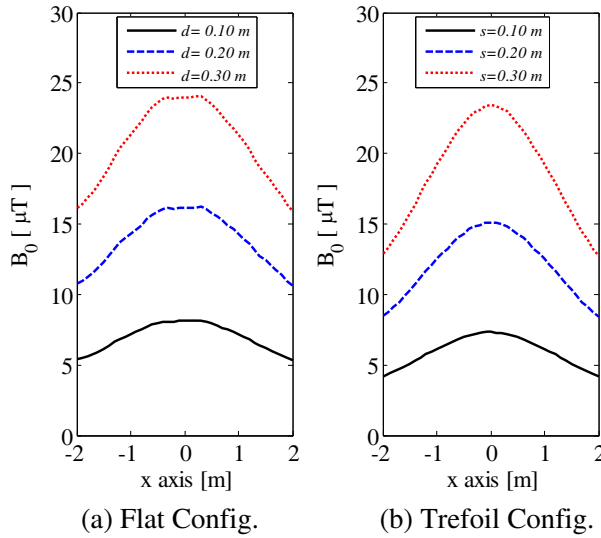


**Figure 5.** Magnetic flux density distribution along the  $x$ -axis at  $h_m = 1\text{ m}$  for several distances between cables. (a) Flat configuration. (b) Trefoil configuration.

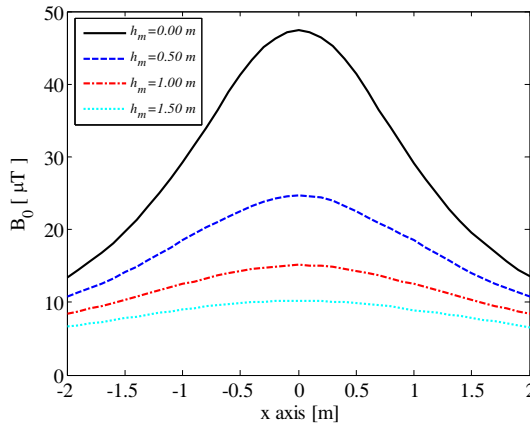


**Figure 6.** Magnetic flux density distribution along the  $x$ -axis for trefoil configuration ( $s = 0.20\text{ m}$ ) at several heights of  $h_m$ .

## 4.2. Shielding with U-shaped Gutters and Cover Plates

### 4.2.1. Influence of Cable Configuration and Shield Material on the Shielding Efficiency and Losses in the Shield

Table 2 shows a comparison of the shielding efficiency and the losses in the shield for several cable configurations and several materials.

**Table 2.** Comparison of cable configuration on losses and shielding efficiency for several shields in the shielding systems.

| Type of shield materi | Cable Config. | $\mu_{r-avg}$ | $B_{avg}$ in shield [Tesla] | $J_{avg}$ in shield [A/m <sup>2</sup> ] | $P_h$ [W/m] | $P_c$ [W/m] | $P_e$ [W/m] | $P$ [W/m] | SE [dB] | Shield cost [€/m] |
|-----------------------|---------------|---------------|-----------------------------|---|-------------|-------------|-------------|-----------|---------|-------------------|
| Aluminium             | Flat          | 1             | $7.17 \times 10^{-4}$       | $3.14 \times 10^5$                      | -           | 20.60       | -           | 20.60     | 23      | 66                |
| Aluminium             | Trefoil       | 1             | $5.49 \times 10^{-4}$       | $2.51 \times 10^5$                      | -           | 13.61       | -           | 13.61     | 20      | 66                |
| DX52                  | Flat          | 354           | 0.12                        | $1.97 \times 10^5$                      | 34.78       | 58.85       | 9.17        | 102.79    | 21      | 43                |
| DX52                  | Trefoil       | 301           | 0.08                        | $1.47 \times 10^5$                      | 15.09       | 26.61       | 5.94        | 47.64     | 17      | 43                |
| Magnetil              | Flat          | 1083          | 0.17                        | $1.72 \times 10^5$                      | 18.32       | 65.90       | 23.06       | 107.28    | 40      | 63                |
| Magnetil              | Trefoil       | 1004          | 0.12                        | $1.19 \times 10^5$                      | 10.06       | 28.16       | 16.04       | 54.26     | 35      | 63                |

\*SE: average of the shielding efficiency along the  $x$ -axis and  $h_m = 1.0$  m

Concerning the shielding efficiency, it is observed that the magnetic shielding efficiency is best for Magnetil, but it is not bad for DX52 and aluminium either. Additionally, the flat configuration gives a better shielding efficiency than the trefoil configuration because the cable position is closer to the shield in the flat configuration, which can be seen in Fig. 7. This gives rise to a higher field, but also to a higher average permeability of the shield material. However, in flat configuration, the induction levels in the observation points are higher in spite of the better shielding efficiency, and also the losses are higher than in trefoil configuration. That leads to the conclusion that the trefoil configuration is the preferred configuration from shielding point of view. The best material is Magnetil.

Concerning the losses, the two ferromagnetic materials are not much different for a given cable configuration, in spite of the high difference in shielding performance. The losses in the Aluminium shield are much lower. When comparing the flat and the trefoil configuration, the flat configuration causes approximately double losses in the ferromagnetic shields. The aluminium shield is preferred when low loss is important.

The material cost is also an important issue to be considered in shielding design. As the power cables may be shielded along hundreds of meters or even kilometers of power line, large quantities of the material will be needed. Hence, the material choice is one of the important issues in terms of shielding cost. The cost of the active material of the shield is given Table 2. Notice that the cost for the shield production and the shield installation in situ are not included. The shields price is given for several materials in euro/ton (price of

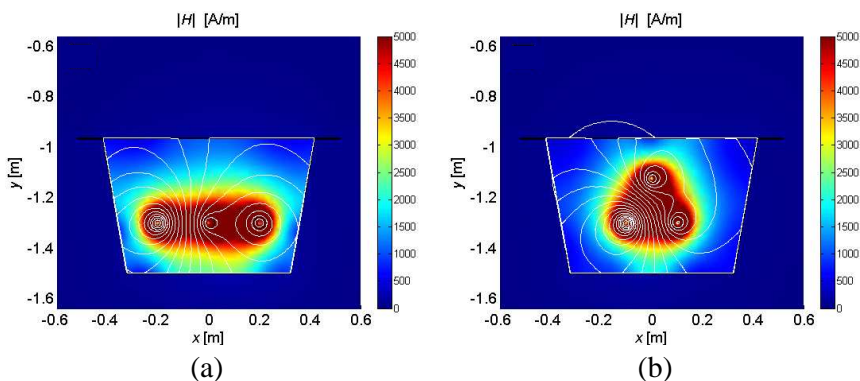


**Figure 7.** An example of magnetic field distribution for (a) the flat configuration, (b) the trefoil configuration at the time instant where  $I_1 = \sqrt{2} \cdot 1500 \sin(\omega t + 0)$ ,  $I_2 = \sqrt{2} \cdot 1500 \sin(\omega t - \pi/3)$ , and  $I_3 = \sqrt{2} \cdot 1500 \sin(\omega t + 2\pi/3)$  A.

December 2010):

- DX52 is a hot-rolled, galvanized material with a price of 500–700 euro/ton. In the computations, we used 600 euro/ton.
- Magnetil has a price of 700–1000 euro/ton<sup>1</sup>. In the computations, we used 850 euro/ton. (<sup>1</sup> Currently, Magnetil is not produced any more by Arcelor-Mittal).
- Aluminium has a price of 2600 euro/ton.

From Table 2, it is clear that DX52 is the cheapest solution.

#### 4.2.2. Influence of Size of the Shield on the Shielding Efficiency and Losses

In order to see the effect of the shield size, we define a scaling parameter  $k$ , which rescales the shield height and width. If we change the scaling parameter, we only change the shield size without touching the other parameters. If  $k = 1$ , all shield dimensions are the same as in Table 1. The shield thickness, the current, and the size and position of the cables are unchanged, and the cable configuration is trefoil. Based on 2D FEM, Fig. 8(a) shows the shielding efficiency versus scaling parameter  $k$ . In Fig. 8(a), and further figures, “shielding efficiency” means the average field reduction on the  $x$ -axis and  $h_m = 1$  m. It is clear that in the ferromagnetic shields, the shielding efficiency improves for lower  $k$  because the permeability is higher for smaller shields: for weak fields, a higher induction leads to a higher permeability: Fig. 3(a). However,

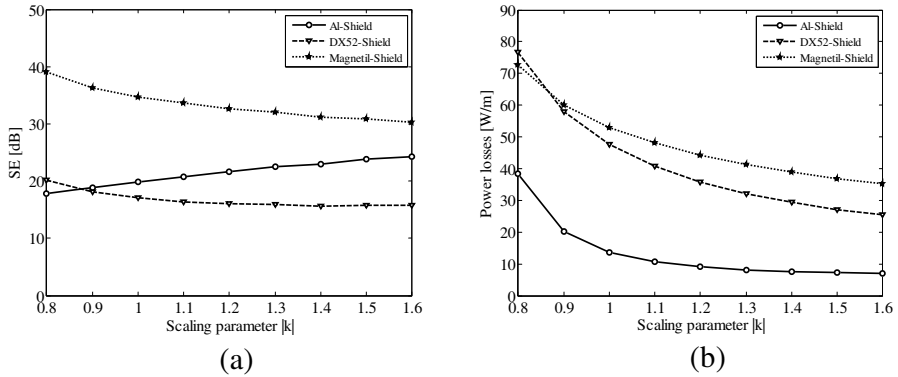


**Figure 8.** (a) Shielding efficiency versus scaling parameter for several materials. (b) Total power losses versus scaling parameter for several materials.

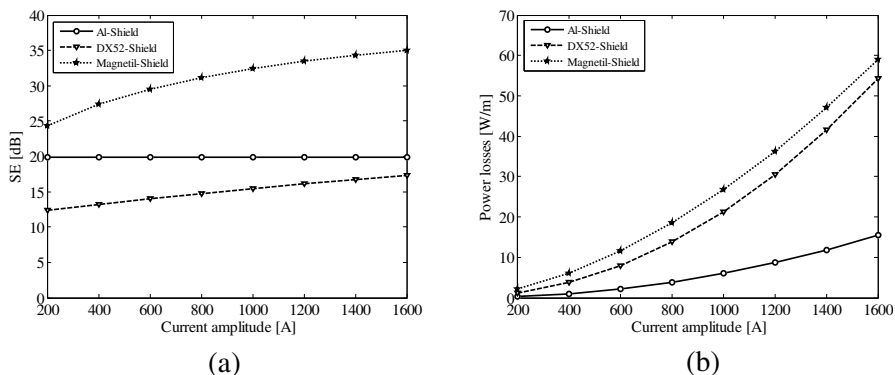
the shielding efficiency increases for the aluminium shield, for higher  $k$  because the enclosed surface increases.

Figure 8(b) shows the total power losses in  $W$  per meter shield length versus the scaling parameter  $k$ . It is clear that in all the shields, larger shields give lower losses because the average induction level decreases with increased shield sizes. For example, the average induction in the DX52 shield for  $k = 0.8$  and  $k = 1.6$  is calculated to be 0.117 T and 0.035 T, respectively.

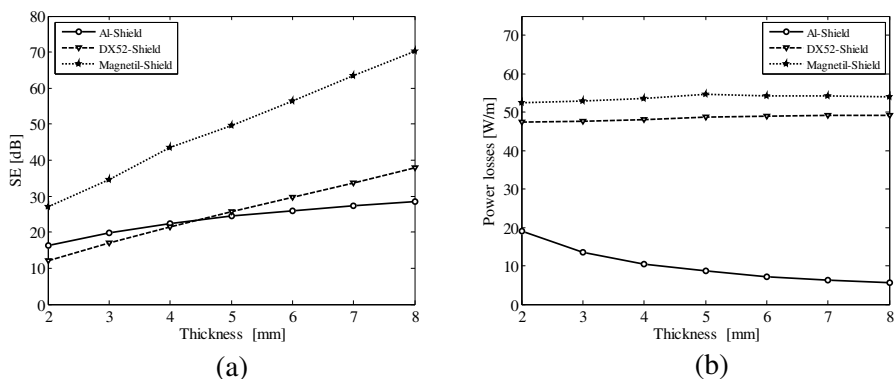
#### 4.2.3. Effect of the Current Amplitude on the Shielding Efficiency and Losses

Figure 9(a) shows the shielding efficiency as a function of the current amplitude in the cables. The shielding efficiency improves with increasing current amplitude for the two electrically conducting and ferromagnetic shielding materials because of the nonlinear magnetic characteristic of the gutters. Indeed, a large part of the shield is in the Rayleigh region (weak fields) where the permeability is lower. Evidently, the shielding factor does not change for the non-ferromagnetic and electrically conducting shielding material (aluminium).

Figure 9(b) shows the total losses in  $W/m$  shield length as a function of the current amplitude in the cables for the considered materials. The power losses are bigger for Magnetil and DX52 than for Aluminium. The losses increase almost quadratically with increasing current amplitude for all the materials.



**Figure 9.** (a) Shielding efficiency versus current amplitude for several materials. (b) Total losses versus current amplitude for several materials.



**Figure 10.** (a) Shielding efficiency versus thickness for several materials. (b) Total losses versus thickness for several materials.

4.2.4. Effect of the Shield Thickness on the Shielding Efficiency and Losses

We have considered the trefoil configuration in this section with  $s = 0.2\text{m}$  and other dimensions given in Table 1. It is evident that the shielding effectiveness improves with increasing material thickness. Fig. 10(a) shows that especially for Magnetil, the increased thickness improves strongly the shielding performance. Although this may seem an incentive to increase the material thickness of 3 mm, the increased cost and weight of the shields are a reason to choose the shield not thicker than necessary. Almost all shields realise 20 dB field reduction, which is sufficient for most applications to comply with the reference

levels of the government.

The losses versus thickness for several materials are shown in  $W/m$  shield length in Fig. 10(b). The losses do almost not change for the ferromagnetic materials with increasing material thickness: as the shield is thicker than the penetration depth, almost no current is flowing in the shielded edge of the thick ferromagnetic shields. The losses decrease with increasing thickness for aluminium, because the current density is reduced. For instance, the averaged current density in the aluminium shield for lower  $t = 2\text{ mm}$  and higher  $t = 8\text{ mm}$  are  $3.73 \times 10^5\text{ A/m}^2$  and  $9.50 \times 10^4\text{ A/m}^2$ , respectively.

## 5. EXPERIMENTAL SETUP, RESULTS AND VALIDATION

In order to verify the simulation results in the previous section, we have made an experimental setup at reduced scale of 1 : 2 illustrated in Fig. 11. The experimental setup consists of a circuit breaker, an adjustable three-phase resistance, a three phase autotransformer, and a special three phase transformer that is connected to the bus-bar cables. The bus-bar cables are short-circuited at the end of the 8 m long HV line in the setup. The resistance and the auto transformer are used to control the balance and the amplitude of the current. In the experimental setup, the three HV cables are copper bars with cross section  $50 \times 5\text{ mm}$ , that carry adjustable balanced three phase currents up to 750 A rms. The shield is 3 mm thick hot rolled galvanized material (ArcelorMittal) has a conductivity and induction dependent permeability given in Section 3 and Fig. 3. The magnetic field measuring system uses a three-axial commercial field meter (accuracy  $\pm 3\%$ , range  $0.01\text{ }\mu\text{T}$  to  $200\text{ }\mu\text{T}$ , and bandwidth from 30 Hz to 2000 Hz).

In order to ensure a good electrical contact between adjacent gutter elements, the conical U-shaped gutters were installed under an axial force causing high contact pressure between overlapping parts. The cover plates were connected to the U-shaped gutters by clips.

Computed and measured magnetic flux density results, distributed along the  $x$ -axis at  $h_m = 0.25\text{ m}$  are shown in Fig. 12. These results validate the computations with the 2D FEM. For instance, we compare in Table 3 the results of this model with measurements of the magnetic flux density and shielding efficiency for both flat and trefoil configurations. In flat configuration, the shielding efficiencies are 18.45 and 18.53 with measurements and 2D FEM, respectively. In trefoil, the obtained shielding efficiencies are 15.13 and 16.37 with measurements and 2D FEM, respectively.

It is observed that — in comparison with the trefoil configuration

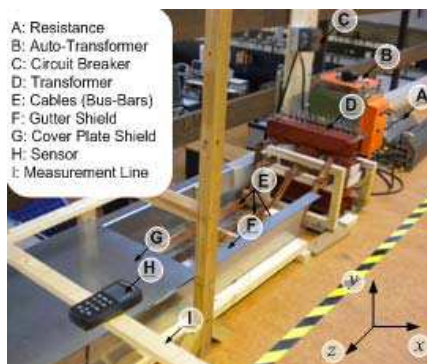
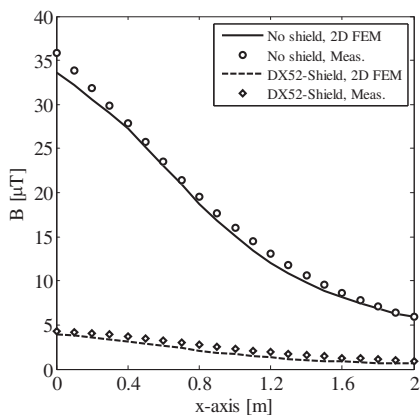
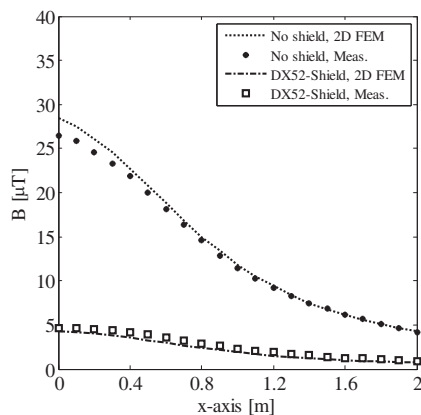


**Figure 11.** Experimental set-up and  $xyz$ -reference frame. The origin of the  $xyz$ -reference frame is at the middle of the bottom of the gutter.



(a) Flat configuration



(b) Trefoil configuration

**Figure 12.** Computed and measured magnetic flux density distribution along the  $x$ -axis at  $H = 1$  m for (a) flat configuration and (b) trefoil configuration.

— the flat configuration results in a significantly higher average induction  $B_0$  in absence of a shield, while the average induction  $B_s$  is slightly lower when the shield is present: the magnetic field in the shield is too low in trefoil configuration to bring the shield in its region of high permeability.

Nevertheless, the flat configuration causes almost double losses: see the loss values in Fig. 13 and Table 4. The classical loss is the dominant component, which is evident because of the 3 mm shield

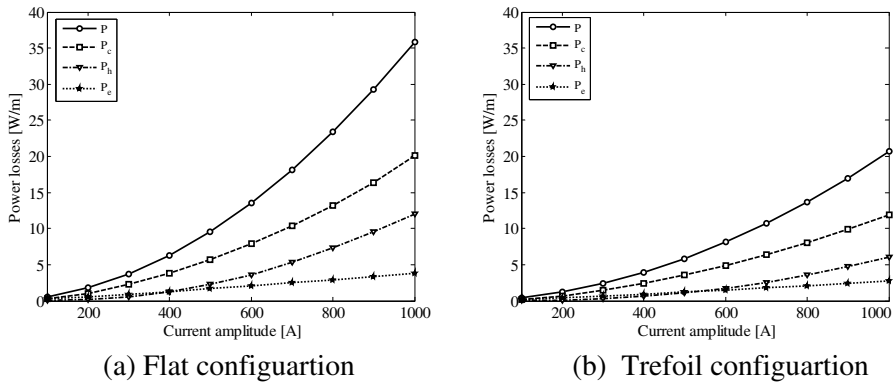


**Figure 13.** Total power losses in W/m for the reduced scale shield in the laboratory setup for (a) flat configuration and (b) trefoil configuration. The loss components are also given: Hysteresis loss  $P_h$ , classical loss  $P_c$  and excess loss  $P_e$ .

**Table 3.** Comparison of measured and simulated results for the two considered cable configurations. The shield is the DX52 shield at reduced scale and the current is 750 A rms per phase.

| Quantity                | Measured results |         | 2D FEM results |         |
|-------------------------|------------------|---------|----------------|---------|
|                         | Flat             | Trefoil | Flat           | Trefoil |
| $B_o$ ( $\mu\text{T}$ ) | 35.80            | 26.44   | 33.63          | 28.45   |
| $B_s$ ( $\mu\text{T}$ ) | 4.28             | 4.69    | 3.98           | 4.32    |
| $SE$ (dB)               | 18.45            | 15.02   | 18.53          | 16.37   |

**Table 4.** Total losses and separated loss components in the reduced scale shield for both flat and trefoil cable configuration.

| Cable configuration | Power Losses (W/m) |       |       |       |
|---------------------|--------------------|-------|-------|-------|
|                     | $P_c$              | $P_h$ | $P_e$ | $P$   |
| Flat                | 6.27               | 2.71  | 11.71 | 20.69 |
| Trefoil             | 3.03               | 1.93  | 7.18  | 12.14 |

thickness. The power loss in the DX52 shield for trefoil configuration is about 40% lower compared to the flat configuration. In case of the trefoil configuration, the losses are 12.14 W/m for a current of 750 A rms per phase.

In order to validate the calculated power losses, Fig. 14 shows the measured and calculated power loss in W/m shield length versus

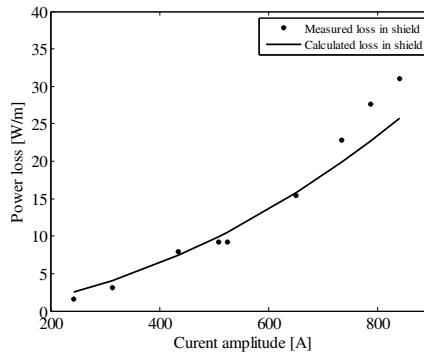


**Figure 14.** Measured and calculated power loss in W/m shield length versus current amplitude.

the busbar current. The power measurements were carried out by a Voltech PM300 power analyzer. The voltage probes were connected to the bus bars between the three-phase supply transformer and the 8 m long shield. Current transformers with a ratio of 169 : 1 were inserted on the busbars, close to the voltage probes. In order to obtain the loss in the shield accurately, the total losses in the busbars were measured with shield present and with shield absent, for identical busbar currents. The losses presented in Fig. 14 are the differences between the corresponding loss values.

## 6. CONCLUSION

The electromagnetic losses and shielding efficiency of shields for a buried three phase high voltage cable are studied with simulations and experiments for several shielding configurations.

For *shielding materials*, the shielding efficiency and the losses are compared for shields with the same geometry: aluminium, and two ferromagnetic steel grades (Magnetil and DX52). From 2D FEM, it is observed that the magnetic shielding efficiency is better for Magnetil (high permeability) than for DX52 (lower permeability) and for aluminium.

Concerning the *cable configuration*, the flat configuration shows a little higher shielding efficiency compared to the trefoil configuration, but nevertheless the remaining field is higher. Moreover, arrangement of the cables in trefoil configuration gives almost 50% lower losses than the flat configuration in the present shielding system. As a result we can say that trefoil configuration is optimum in the shielding system because of lower losses and adequate shielding efficiency.

The *shield size* has a relatively small effect on the shielding: a larger shield slightly decreases the shielding efficiency for the ferromagnetic shields, and increases it for aluminum. However, the losses strongly decrease with increasing size, because the average induction level is much weaker in a large shield.

As a function of the *current amplitude*, the shielding efficiency is constant for aluminum, but it increases for the ferromagnetic shields because their average permeability increases. The losses increase almost quadratically with increasing current amplitude for all materials.

With increasing *shield thickness*, the shielding effectiveness improves without causing higher losses.

The over-all conclusion is that:

If the best shielding effectiveness for a given thickness is required, a high permeability material like Magnetil is preferred.

If a low cost per meter shield is required, a ferromagnetic grade with lower permeability can be used.

If low magnetic losses in the shield are important, aluminum is preferred.

## ACKNOWLEDGMENT

This work was supported by the Scientific and Technological Research Council of Turkey (TUBITAK) and by the IAP project P6/21 of the Belgian government. P. Sergeant is a postdoctoral researcher for the "Fund of Scientific Research Flanders" (FWO).

## REFERENCES

1. Banfai, B., G. G. Karady, C. J. Kim, and K. B. Maracas, "Magnetic field effects on CRT computer monitors," *IEEE Transactions on Power Delivery*, Vol. 15, No. 1, 307–312, 2000.
2. Santoro, N., A. Lisi, D. Pozzi, E. Pasquali, A. Serafino, and S. Grimaldi, "Effect of extremely low frequency (ELF) magnetic field exposure on morphological and biophysical properties of human lymphoid cell line (Raji)," *Biochimica et Biophysica Acta*, Vol. 1357, 281–290, 1997.
3. Villeneuve, P. J., D. A. Agnew, K. C. Johnson, Y. Maa, and the Canadian Cancer Registries Epidemiology Research Group, "Brain cancer and occupational exposure to magnetic fields among men: Results from a Canadian population-based case-control study," *International Journal of Epidemiology*, Vol. 31, No. 1, 210–217, 2002.

4. 2004/40/EC, "Directive of the European Parliament and of the Council of 29th April 2004 on the minimum health and safety requirements regarding the exposure of workers to the risks arising from physical agents (electromagnetic fields)," *Official Journal of the EU*, No. L184, 1–9 May 24, 2004, [<http://www.hse.gov.uk/radiation/nonionising/l184emf.pdf>], accessed Mar. 21, 2011].
5. Habiballah, I. O., A. S. Farag, M. M. Dawoud, and A. Firoz, "Underground cable magnetic field simulation and management using new design configurations," *Electric Power Systems Research*, Vol. 45, 141–148, 1998.
6. Dawoud, M. M., I. O. Habiballah, A. S. Farag, and A. Firoz, "Magnetic field management techniques in transmission underground cables," *Electric Power Systems Research*, Vol. 48, 177–192, 1999.
7. López, J. C. P. and P. C. Romero, "The effectiveness of compensated passive loops for mitigating underground power cable magnetic fields," *IEEE Transactions on Power Delivery*, Vol. 99, 1–10, 2010.
8. Faghihi, F. and H. Heydari, "Reduction of leakage magnetic field in electromagnetic systems based on active shielding concept verified by eigenvalue analysis," *Progress In Electromagnetics Research*, Vol. 96, 217–236, 2009.
9. Sergeant, P., L. Dupré, and J. Melkebeek, "Magnetic shielding of buried high voltage cables by conductive metal plates," *COMPEL*, Vol. 27, No. 1, 170–180, 2008.
10. Zucca, M., G. Lorusso, F. Fiorillo, P. E. Roccatò, and M. Annibale, "Highly efficient shielding of high-voltage underground power lines by pure iron screens," *J. Magn. Magn. Mater.*, Vol. 320, 1065–1069, 2008.
11. De Wulf, M., P. Wouters, P. Sergeant, L. Dupré, E. Hoferlin, S. Jacobs, and P. Harlet, "Electromagnetic shielding of high-voltage cables," *J. Magn. Magn. Mater.*, Vol. 316, 908–911, 2007.
12. Xu, X.-B. and G. Liu, "Investigation of the magnetic field produced by unbalanced phase current in an underground three-phase pipe-type cable," *Electric Power Systems Research*, Vol. 62, 153–160, 2002.
13. Koroglu, S., P. Sergeant, R. Sabariego, V. D. Quoc, and M. D. Wulf, "Influence of contact resistance on shielding efficiency of shielding gutters for HV cables," *14th Biennial IEEE Conference on Electromagnetic Field Computation*, Chicago, USA, May 9–12, 2010.

14. Xu, X. and X. Yang, "A hybrid formulation based on unimoment method for investigating the electromagnetic shielding of sources within a steel pipe," *Progress In Electromagnetics Research*, Vol. 12, 133–157, 1996.
15. Kuang, J. and S. A. Boggs, "Pipe-type cable losses for balanced and unbalanced currents," *IEEE Transactions on Power Delivery*, Vol. 17, No. 2, 313–317, 2002.
16. Moutassem, W. and G. J. Anders, "Calculation of the eddy current and hysteresis losses in sheathed cables inside a steel pipe," *IEEE Transactions on Power Delivery*, Vol. 25, No. 4, 2054–2063, 2010.
17. Bertotti, G., *Hysteresis in Magnetism*, Academic Press, San Diego, 1998.
18. Bertotti, G., "General properties of power losses in soft ferromagnetic materials," *IEEE Transactions on Magnetics*, Vol. 24, No. 1, 621–630, 1988.
19. Dupré, L., G. Bertotti, V. Basso, F. Fiorillo, and J. Melkebeek, "Generalisation of the dynamic preisach model toward grain oriented Fe-Si alloys," *Physica B: Condensed Matter*, Vol. 275, No. 1–3, 202–206, 2000.
20. Permiakov, V., L. Dupré, A. Pulnikov, and J. Melkebeek, "Loss separation and parameters for hysteresis modelling under compressive and tensile stresses," *J. Magn. Magn. Mater.*, Vol. 272–276, 553–554, 2004.